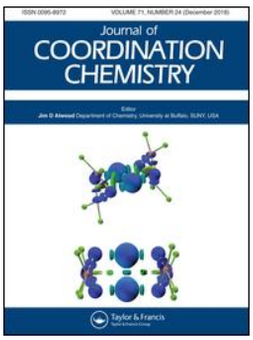

Taylor & Francis
Taylor & Francis Group

Journal of Coordination Chemistry

ISSN: (Print) (Online) Journal homepage: https://www.tandfonline.com/loi/gcoo20

Anchoring of a terpyridine-based Mo(VI) complex on manganese ferrite as a recoverable catalyst for epoxidation of olefins under solvent-free conditions

Mahsa Fadaei Sarabi, Abolfazl Bezaatpour & Ali Mahmoudi

To cite this article: Mahsa Fadaei Sarabi, Abolfazl Bezaatpour & Ali Mahmoudi (2021): Anchoring of a terpyridine-based Mo(VI) complex on manganese ferrite as a recoverable catalyst for epoxidation of olefins under solvent-free conditions, Journal of Coordination Chemistry, DOI: 10.1080/00958972.2021.1904507

To link to this article: https://doi.org/10.1080/00958972.2021.1904507

Published online: 24 Mar 2021.

JOURNAL OF COORDINATION CHEMISTRY
https://doi.org/10.1080/00958972.2021.1904507

Taylor & Francis
Taylor & Francis Group

Anchoring of a terpyridine-based Mo(VI) complex on manganese ferrite as a recoverable catalyst for epoxidation of olefins under solvent-free conditions

Mahsa Fadaei Sarabi[a], Abolfazl Bezaatpour[b] and Ali Mahmoudi[a]

[a]Faculty of Science, Department of Chemistry, Islamic Azad University North Tehran Branch, Tehran, Iran; [b]Faculty of Basic Science, Department of Chemistry, University of Mohaghegh Ardabili, Ardabil, Iran

ABSTRACT

A magnetically separable heterogeneous nanocatalyst was obtained by anchoring a terpyridine-based Mo(VI) complex on modified $MnFe_2O_4$ nanoparticles and characterized by Fourier transform infrared (FT-IR), X-ray diffraction (XRD) and diffuse reflectance spectroscopies (DRS), transmission electron microscopy (TEM), scanning electron microscopy (SEM), vibrating sample magnetometry (VSM), X-ray photoelectron spectroscopy (XPS) and Brunauer-Emmett-Teller (BET) analysis. The catalytic activity of the supported molybdenum based catalyst was evaluated in the selective epoxidation of various olefins (cyclooctene, limonene, 1-dodecane, 1-heptene, styrene, 1-indene, α-pinene, cyclohexene) with *tert*-butyl hydroperoxide (TBHP) as an oxidant under solvent-free conditions. This nanocatalyst was easily separated by using an external magnetic field and reused consecutively at least five times with no significant loss in selectivity and catalytic activity. The short reaction time, simple preparation, high conversion, good physicochemical stability and magnetic recycling of the catalysts are beneficial.

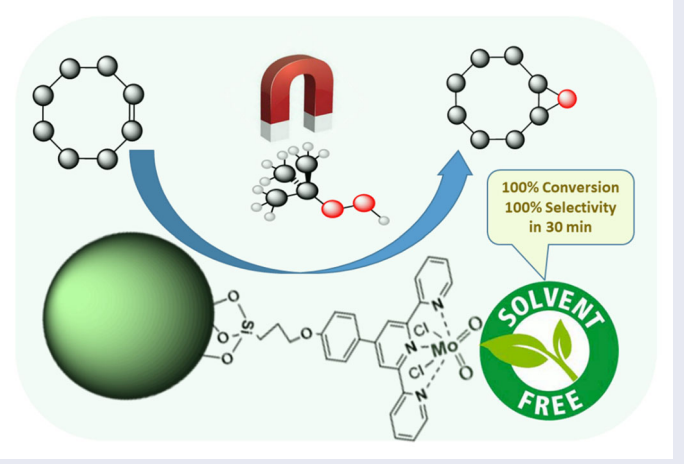

ARTICLE HISTORY
Received 31 August 2020
Accepted 8 February 2021

KEYWORDS
Epoxidation; olefins; molybdenum; magnetically; $MnFe_2O_4$

CONTACT Abolfazl Bezaatpour a_Bezaatpour@Yahoo.com Faculty of Basic Science, Department of Chemistry, University of Mohaghegh Ardabili, Ardabil, Iran.

1. Introduction

Epoxidation of olefins is a principal reaction to obtain epoxides which play an essential role in pharmaceutical, epoxy resins production, cosmetics, and also plasticizers industries [1]. Various types of supported catalysts by loading Mo(VI) complexes on different supports, such as silica [2], graphene, multiwall carbon nanotubes [3] and metal oxides [4] have been reported in epoxidation of olefins. Schiff base complexes of Mo(VI) have been extensively applied as a favorable homogeneous catalyst for epoxidation of alkenes due to properties including facile preparation, stability, and commercial accessibility [5–7]. Preparation of these complexes from inexpensive materials such as MoO_3 is a major advantage of these complexes [7–9]. Although homogeneous catalysts are commonly used for epoxide production, difficult separation of these catalysts from the reaction mixture and subsequent environmental pollution limits further application [10, 11]. To solve this serious problem, heterogeneous catalysts by supporting a catalyst on nanoparticles have been widely developed [12]. Magnetic nanoparticles have been extensively used in immobilization of metal nanoparticles. Among different kinds of nanoparticles, magnetic nanoparticles such as Fe_3O_4, $MnFe_2O_4$ and $MgFe_2O_4$ have attracted attention due to their ease of separation, nontoxicity, high surface area and more importantly high physicochemical stability [13, 14]. Surface functionalization of various magnetic nanoparticles is an approach for synthesis of magnetically separable heterogeneous catalysts [15, 16].

Solvent-less reactions offer many benefits in environmental protection, saving in labor, lowering costs, and chemical waste reduction [17–19]. Application of *tert*-butyl hydroperoxide (TBHP) as an eco-friendly oxidant in epoxidation is widely reported [20–22]. The advantages of TBHP over H_2O_2 include thermal stability, selectivity, low cost and its safety [23].

Following our previous attempts to investigate catalytic epoxidation of olefins by Schiff base complex supported nanocatalysts [24–27], herein we present the anchoring of a terpyridine based Mo(VI) complex onto the surface of chloro-modified magnetic manganese ferrite nanoparticles. Complete characterization of the new heterogeneous nanocatalyst ($MnFe_2O_4$@Phttpy-MoO_2) was carried out via FT-IR, XRD, BET, SEM, EDX, TEM, VSM, and also XPS analysis. Additionally, the catalytic activity of $MnFe_2O_4$@Phttpy-MoO_2 was assessed for green and selective epoxidation of several olefins. It was noticed that the obtained $MnFe_2O_4$@Phttpy-MoO_2 nanocatalyst could be applied and recycled many times without apparent conversion reduction.

2. Experimental

2.1. Materials and instruments

Manganese chloride ($MnCl_2{\cdot}4H_2O$), ferric chloride ($FeCl_3{\cdot}6H_2O$), 4-hydroxybenzaldehyde, toluene, 2-acetylpyridine, ammonia (25% w/w), hydrogen peroxide, urea hydrogen peroxide (UHP), cyclooctene, limonene, 1-dodecane, 1-heptene, styrene, 1-indene, α-pinene, cyclohexene, MoO_3 and all other chemicals were obtained from Merck chemical company (Germany). *tert*-Butyl hydroperoxide (TBHP) and 3-

chloropropyl)triethoxysilane (CPTES) were purchased from Sigma-Aldrich. All chemicals were used without purification.

Fourier transform infrared (FT-IR) spectra were obtained as KBr disks on a Shimadzu 8400S spectrophotometer. Diffuse reflectance spectroscopy measurements were carried out using a Scinco 4100 UV-Vis diffuse spectrophotometer within the 200-900 nm range applying $BaSO_4$ as reference material. An X-ray diffractometer (Philips X'Pert 1, Netherlands) equipped with Cu-Kα radiation was applied for obtaining X-ray diffraction patterns of products. BET analysis was performed using a BELSORP Mini II analyzer. The surface morphology and mean particle size of nanoparticles were studied with LEO 1430 VP scanning electron microscopy (SEM). Transmission electron microscopy (TEM) micrographs were recorded via a Philips CM120 microscope. The magnetic properties of products were characterized by a Meghnatis Daghigh Kavir Co., Kashan Kavir vibrating sample magnetometer (VSM). Monitoring of the oxidation products was carried out by an Agilent 7890 A gas chromatograph equipped with a flame-ionization detector (FID) and capillary column.

2.2. Preparation of $MnFe_2O_4$@Si-$(CH_2)_3$-Cl

$MnFe_2O_4$ nanoparticles were synthesized according to the literature [28]. In brief, an aqueous solution of $MnCl_2{\cdot}4H_2O$ and $FeCl_3{\cdot}6H_2O$ containing Mn^{2+} (0.01 M) and Fe^{3+} (0.2 M) were prepared and then added slowly into 100 mL NaOH (3 M) at 95 °C. After continuous stirring for 2 h, the precipitate was collected, washed three times with deionized water and calcined at 60 °C for 12 h. First 2 g of the as-prepared $MnFe_2O_4$ nanoparticles were dispersed in toluene (100 mL) under ultrasonication and then CPTES (5 mL) was added dropwise and refluxed for 48 h. The $MnFe_2O_4$@Si-$(CH_2)_3$-Cl particles were washed with DI water and ethanol and dried at 80 °C for 24 h.

2.3. Synthesis of 4-(4-hydroxyphenyl)-2,2: 6, 2-terpyridine (4-OH-Phttpy)

4-(4-Hydroxyphenyl)-2,2:6,2-terpyridine was prepared according to Oyetade *et al.* [29]. Into a 2:1 (v/v) mixture of water and ethanol (15 mL), 2-acetylpyridine (2.424 g) and 4-hydroxybenzaldehyde (1.221 g) were added. After that, NaOH pellets (1.458 g) and NH_3 (30 mL) were added and stirred for 8 h at room temperature until a creamy precipitate was obtained. After filtration, the resulting solid was washed with deionized water and ethanol to achieve the white product.

2.4. Preparation of $MnFe_2O_4$@Si-$(CH_2)_3$-O-Phttpy

A solution of 4-(4-hydroxyphenyl)-2,2:6,2-terpyridine was added to a suspension of $MnFe_2O_4$@Si-$(CH_2)_3$-Cl (0.5 g in 40 mL DMF). Then, the mixture was stirred and refluxed for 72 h at 100 °C. The obtained $MnFe_2O_4$@Si-$(CH_2)_3$-O-Phttpy was recovered by a magnet and washed with DMF and water repeatedly.

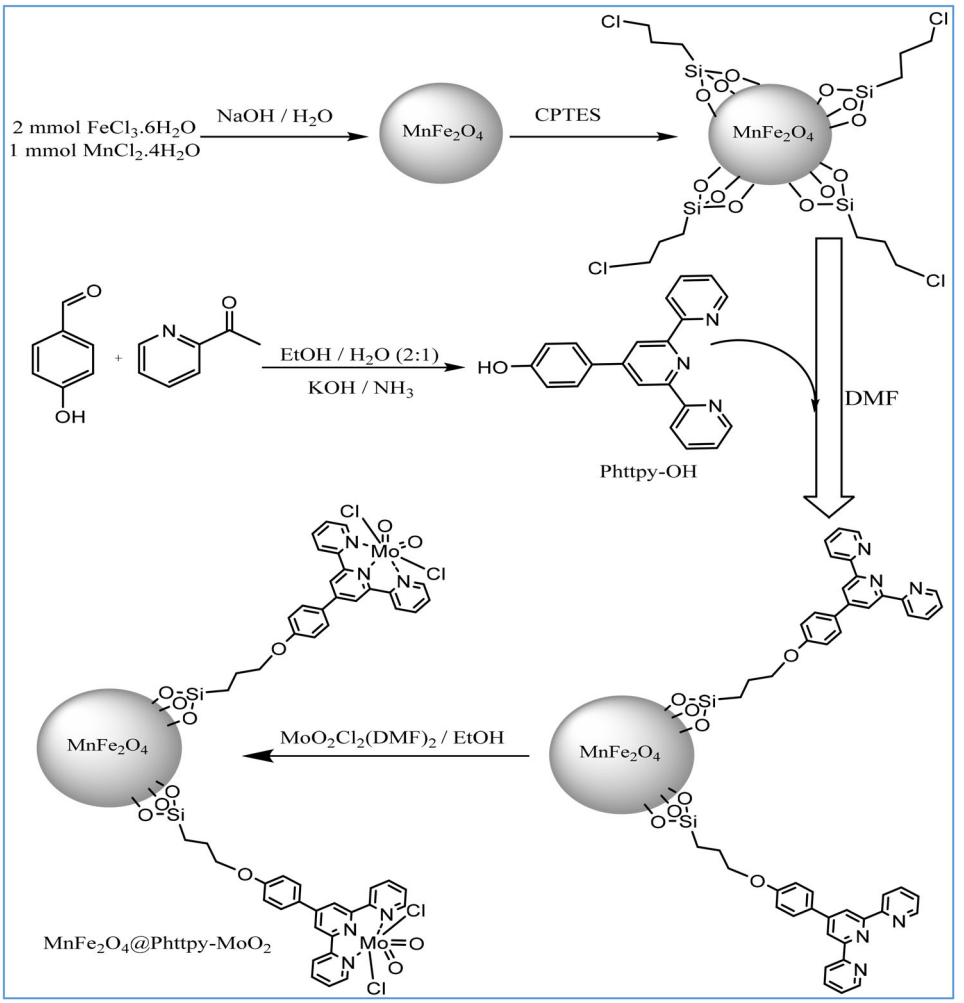

Scheme 1 Proposed preparation pathway for $MnFe_2O_4$@Phttpy-MoO_2 heterogeneous nanocatalyst.

2.5. Preparation of $MnFe_2O_4$@Phttpy-MoO_2

$MoO_2Cl_2(DMF)_2$ was synthesized according to the method described [30]. Initially, ethanolic solution of $MoO_2Cl_2(DMF)_2$ (1.96 g) was added drop by drop to a suspension of $MnFe_2O_4$@Si-$(CH_2)_3$-O-Phttpy (2.0 g in 50 mL ethanol). In the next step, the reaction mixture was refluxed for 24 h at 100 °C. Finally, separation of the as-prepared catalyst was performed using an external magnet and washed four times with DI water and ethanol.

2.6. Catalytic activity

The catalytic activity of $MnFe_2O_4$@Phttpy-MoO_2 was evaluated for epoxidation of various alkenes. Typically 0.005 mg (3.64×10^{-4} mmol determined based on XPS data) of $MnFe_2O_4$@Phttpy-MoO_2, chlorobenzene as internal standard (0.5 mmol), alkenes

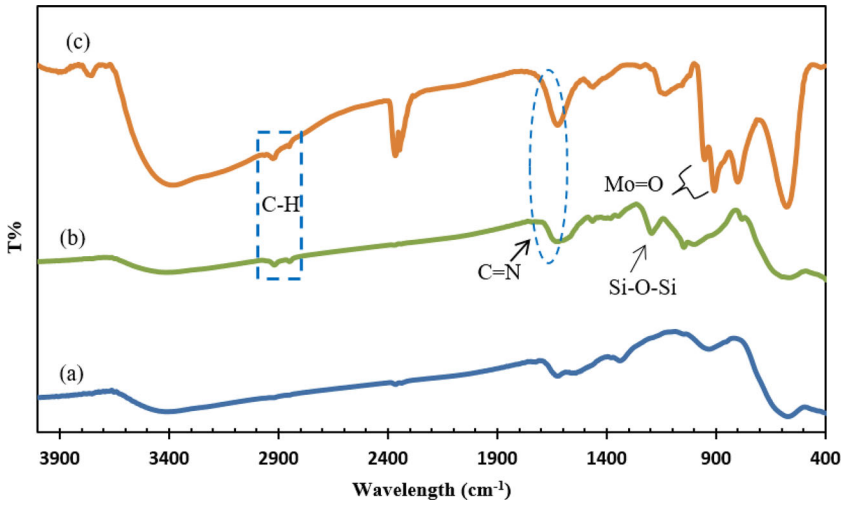

Figure 1. FT-IR spectra of (a) $MnFe_2O_4$ NPs, (b) $MnFe_2O_4$@Si-$(CH_2)_3$-O-Phttpy and (c) $MnFe_2O_4$@Phttpy-MoO_2.

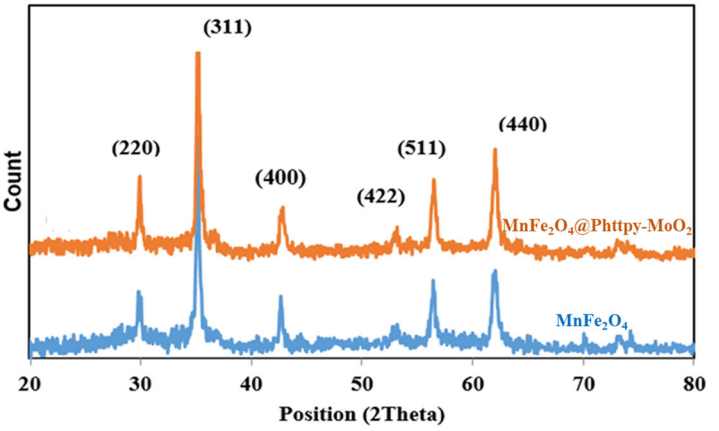

Figure 2. XRD patterns of $MnFe_2O_4$ NPs and $MnFe_2O_4$@Phttpy-MoO_2.

(0.5 mmol) and TBHP (2 mmol) were added to the catalytic reactor. The catalytic reactor was stirred at 95 °C under solvent-free conditions and the oxidation products were monitored by gas chromatography (FID).

3. Results and discussion

3.1. Characterization of catalyst

The preparation of $MnFe_2O_4$@Phttpy-MoO_2 nanocatalyst is presented in Scheme 1. Initially, the magnetic $MnFe_2O_4$ nanoparticles were prepared by a chemical co-precipitation route. Then the magnetic nanoparticles were modified with Phttpy-MoO_2. To confirm the preparation of $MnFe_2O_4$@Phttpy-MoO_2, FT-IR analysis was applied. Figure

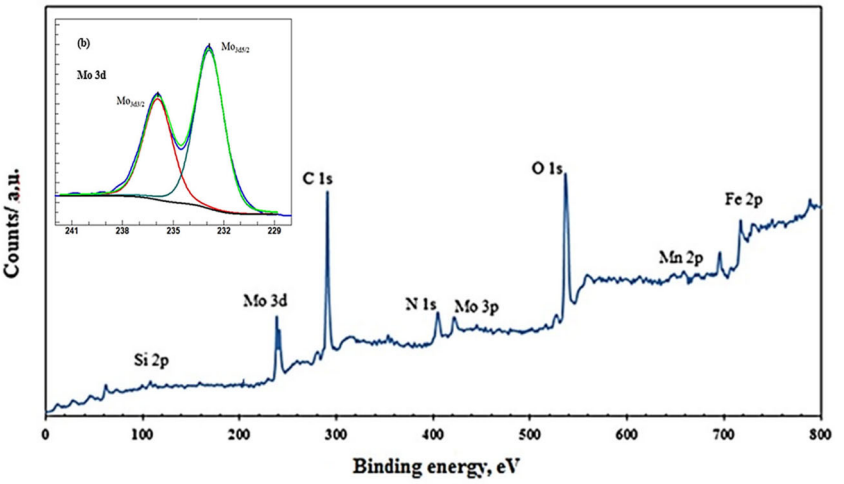

Figure 3. XPS spectrum of (a) $MnFe_2O_4$@Phttpy-MoO_2 and core level spectra of Mo3d.

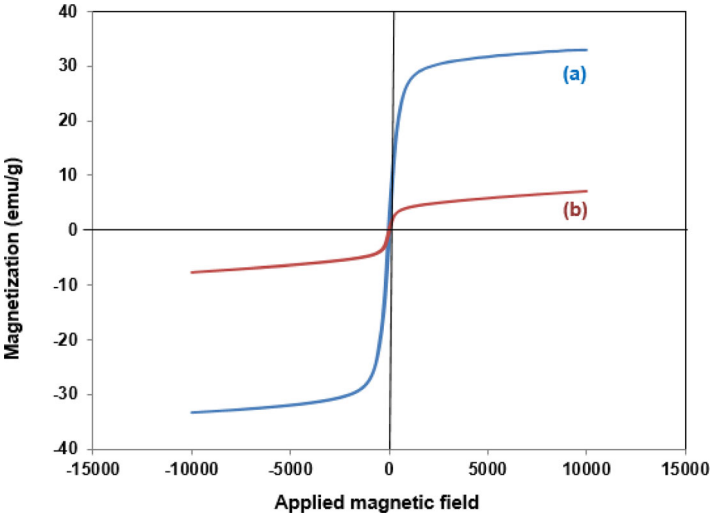

Figure 4. (a) VSM graph of $MnFe_2O_4$ and (b) $MnFe_2O_4$@Phttpy-MoO_2.

1 shows the FT-IR spectra of $MnFe_2O_4$ nanoparticles, $MnFe_2O_4$@Si-$(CH_2)_3$-O-Phtpy and $MnFe_2O_4$@Phttpy-MoO_2. As depicted in Figure 1(a), bands at 495 and 675 cm^{-1} are assigned to Mn-O and Fe-O stretching modes of manganese ferrite nanoparticles [31]. The $MnFe_2O_4$@Si-$(CH_2)_3$-O-Phttpy sample (Figure 1(b)) shows additional vibrations of the C = N band at 1626 cm^{-1}. In Figure 1(b), the absorption at 1114 cm^{-1} is related to Si-O-Si vibrations. The two adjacent bands at 918 and 945 cm^{-1} in Figure 1(c) are attributed to the presence of *cis* O = Mo = O group in the supported catalyst [32].

Figure 2 reveals the X-ray powder diffraction patterns of $MnFe_2O_4$ and $MnFe_2O_4$@Phttpy-MoO_2. The emergence of diffraction peaks at $2\Theta = 30.07$, 35.17, 43.72, 53.27 and 56.47 were related to the Bragg reflections of (211), (311), (400), (422), (511), and (440) planes, respectively. The obtained characteristic diffraction peaks in Figure 2 are assigned to the cubic centered geometry of manganese ferrite

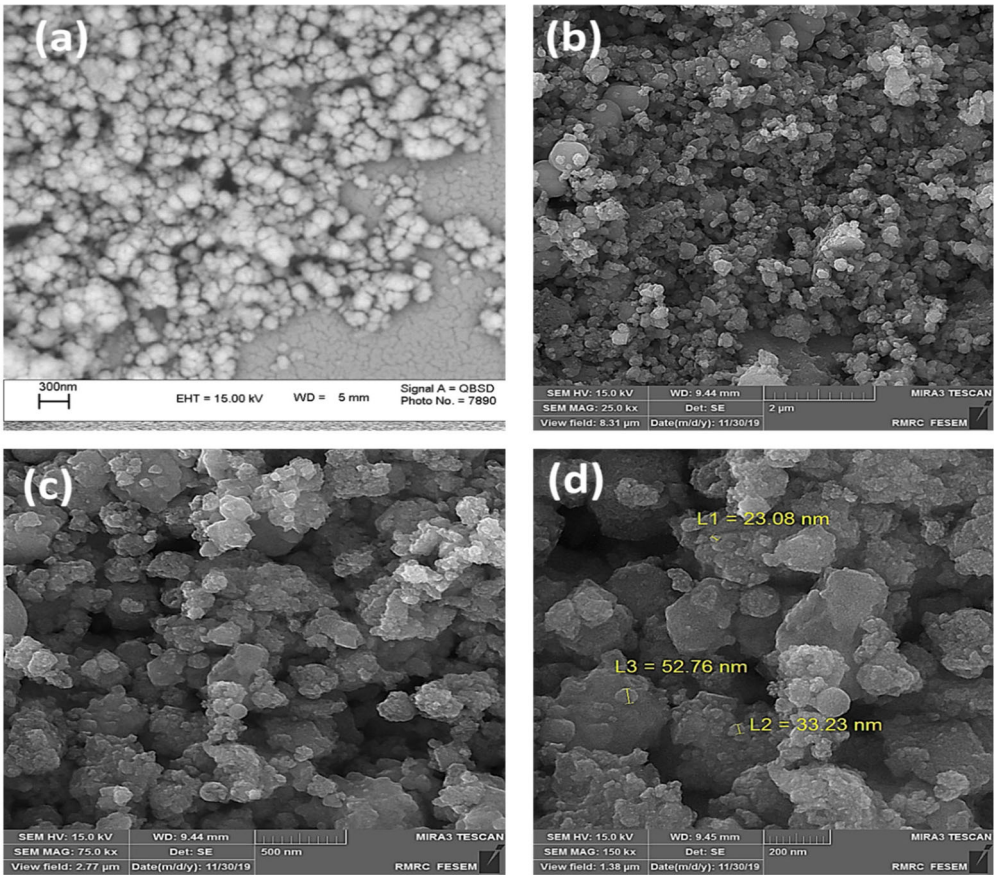

Figure 5. FE-SEM micrographs of (a) $MnFe_2O_4$ NPs and $MnFe_2O_4$@Phttpy-MoO_2 in (b) 2 µm, (c) 500 nm and (d) 200 nm.

nanoparticles in accord with standard JCPDS card NO. 74-2403. The particle size of $MnFe_2O_4$@Phttpy-MoO_2 was estimated at 32 nm by using the Debye-Scherrer equation ($L = K\lambda/\beta.\cos\theta$). Here $\lambda(= 0.154\,nm)$ is the wavelength of X-ray, θ is the diffraction angle (= 17.61) of (311) crystal plane and K is a constant usually 0.94, FWHM is 0.28 in degree and β is 0.00488 in radian.

The X-ray photoelectron spectrum (XPS) was employed to further identify the chemical composition and chemical states of $MnFe_2O_4$@Phttpy-MoO_2 (Figure 3). The bands at 100 eV (Si2p), 234 eV (Mo3d), 296 eV (C1s), 400 (N1s), 414 (Mo3p) and 546 (O1s) were assigned giving the atomic percentage for N, 2.3; O, 7.3; Fe, 1.4 and Mo, 0.7, confirming that the terpyridine-based complex of dioxo-Mo(VI) was immobilized onto the $MnFe_2O_4$ surface. The Mo3d core level spectrum can be deconvolved into two peaks at 232.90 and 235.85 eV, attributable to $Mo3d_{5/2}$ and $Mo3d_{3/2}$, respectively.

A vibration sample magnetometer (VSM) was applied to evaluate the magnetic characteristics of the prepared samples. Figure 4 shows that saturation magnetization for $MnFe_2O_4$ and $MnFe_2O_4$@Phttpy-MoO_2 is obtained at 32.97 and 7.13 emu g^{-1}, respectively. Furthermore, no hysteresis loop was observed in magnetization curves, which indicates superparamagnetic behavior of the synthesized magnetic $MnFe_2O_4$

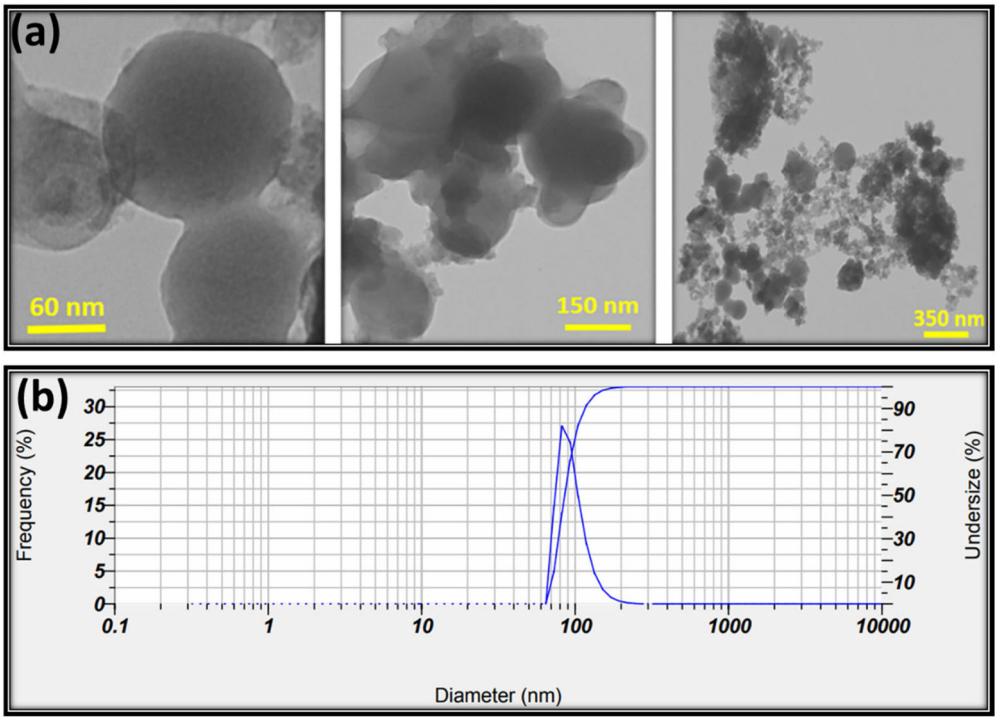

Figure 6. (a) Transmission electron microscopy image of $MnFe_2O_4$@Phttpy-MoO_2; (b) DLS results of $MnFe_2O_4$@Phttpy-MoO_2.

NPs. The results indicate immobilization of catalyst on magnetic NPs decreases magnetic saturation, but it is still enough to remove $MnFe_2O_4$@Phttpy-MoO_2 from solution by applying an external magnetic field.

The surface morphology and particle size of $MnFe_2O_4$@Phttpy-MoO_2 were studied via scanning electron microscopy. As illustrated in Figure 5, the magnetic catalyst was composed of aggregated spherical particles. Also, the size distribution and shape of the prepared supported catalyst was investigated using transmission electron microscopy. Figure 6 shows the TEM image and DLS analysis of $MnFe_2O_4$@Phttpy-MoO_2. Figure 6(a) depicts TEM micrographs of magnetic $MnFe_2O_4$@Phttpy-MoO_2 nanocatalyst, showing uniform spherical nanoparticles obtained with an average diameter of 23-50 nm. There may be two reasons for the difference in catalyst size obtained through the Debye-Scherrer equation and TEM. One is the particles aggregation and the second is that the Debye-Scherrer equation shows only an approximate size of the crystalline phase of $MnFe_2O_4$ and does not evaluate the modification layer on the $MnFe_2O_4$. As shown in Figure 6(b), the DLS measurements performed on $MnFe_2O_4$@Phttpy-MoO_2 suspensions showed hydrodynamic radius of particles about 79 nm.

The EDAX spectra (Figure 7) of catalyst provide clear evidence for presence of Mn (4.71%), Mo (1.19%,), Fe (11.42%), Si (1.11%), N (3.21%) and C (24.32%), consistent with the chemical composition of the catalyst. Also, the EDX mapping mode (Figure 7) showed that all elements were well distributed on the $MnFe_2O_4$@Phttpy-MoO_2 nanocatalyst.

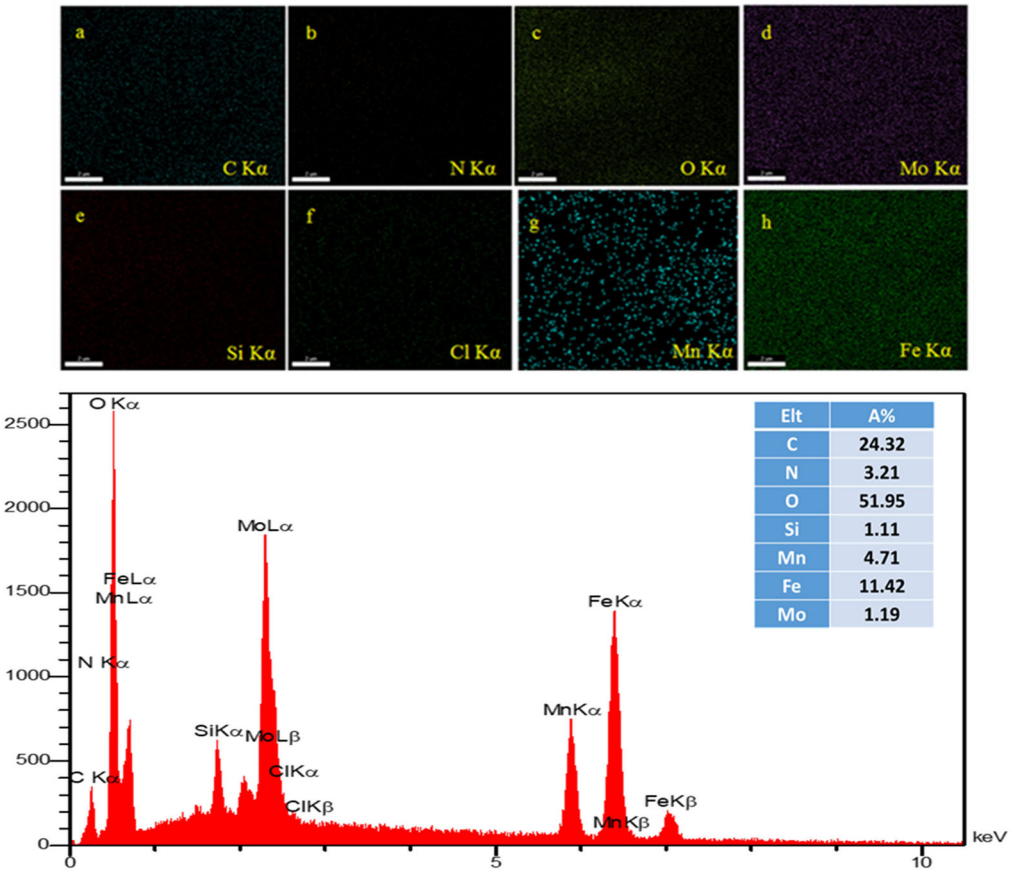

Figure 7. EDX spectrum and mapping micrographs of (a) C, (b) N, (c) O, (d) Mo, (e) Si, (f) Cl, (g) Mn and (h) Fe of $MnFe_2O_4$@Phttpy-MoO_2.

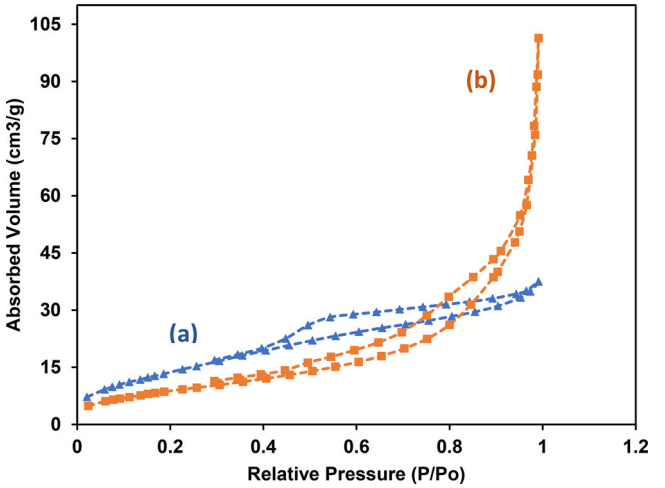

Figure 8. N_2 adsorption-desorption isotherms of (a) $MnFe_2O_4$ NPs and (b) $MnFe_2O_4$@Phttpy-MoO_2 nanocatalyst.

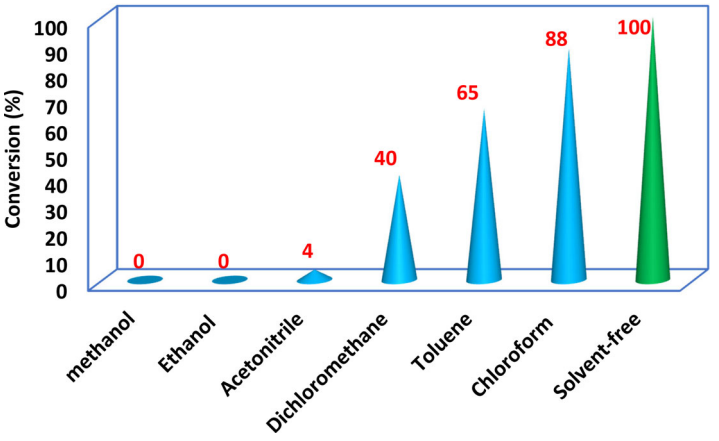

Figure 9. Oxidation of cyclooctene (0.5 mmol) in various solvents (5 mL) and under solvent-free conditions at 95 °C during 30 min, TBHP (1.5 mmol), $MnFe_2O_4$@Phttpy-MoO_2 (3.64×10^{-4} mmol).

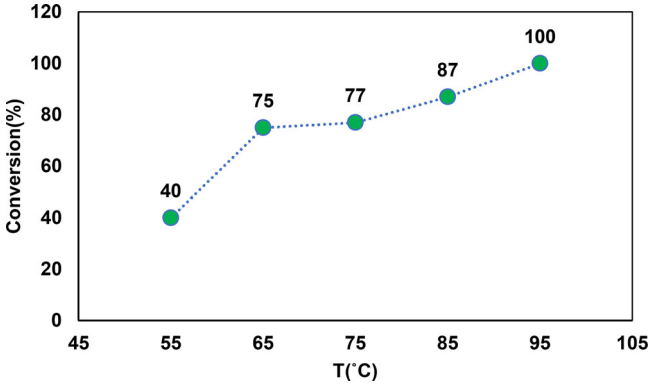

Figure 10. Effect of temperature on epoxidation of cyclooctene (0.5 mmol) with TBHP (1.5 mmol) under solvent-free conditions during 30 min, catalyst (3.64×10^{-4} mmol).

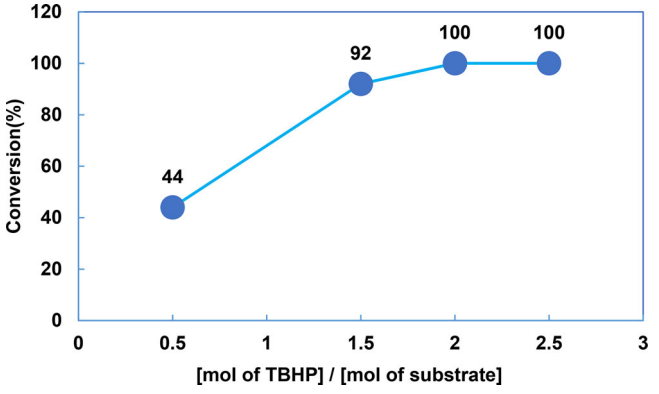

Figure 11. Effect of [TBHP]/[cyclooctene] ratio on epoxidation process at 95 °C under solvent-free conditions during 30 min, catalyst (3.64×10^{-4} mmol).

Table 1. Catalytic oxidation of different olefins by $MnFe_2O_4$@Phttpy-MoO_2 under solvent-free conditions[a].

Alkenes	Time	Oxidant	% conversion	% Selectivity	TOF $[h^{-1}]$[b]
Cyclooctene	30 min	TBHP	99	100	2719
	60 min	TBHP	90	100	1236[c]
	60 min	$NaIO_4$	0.0	–	–
	60 min	H_2O_2	0.0	–	–
	60 min	UHP	0.0	–	–
Limonene	30 min	TBHP	99	63[d]	2719
1-dodecene	30 min	TBHP	92	100	2527
1-heptene	60 min	TBHP	67	100	920
Styrene	30 min	TBHP	95	62[e]	2609
1-indene	60 min	TBHP	54	60[f]	741
α-Pinene	60 min	TBHP	96	100	1318
Cyclohexene	60 min	TBHP	95	100	1304

[a]Catalytic reaction condition: solvent-free; catalyst $= 3.64 \times 10^{-4}$; 0.5 mmol alkene;.
[b]Calculated as [mmol of epoxide]/[mmol of catalyst]×time (h).
[c]Hot leaching test was studied of catalyst leaching in epoxidation of cyclooctene.
[d]1,2-Limonene oxide is the desired product and 1,2,8,9-limonene dioxide is a byproduct.
[e]Styrene oxide is the desired product and acetophenone is the other one.
[f]1H-inden-1-one 40%.

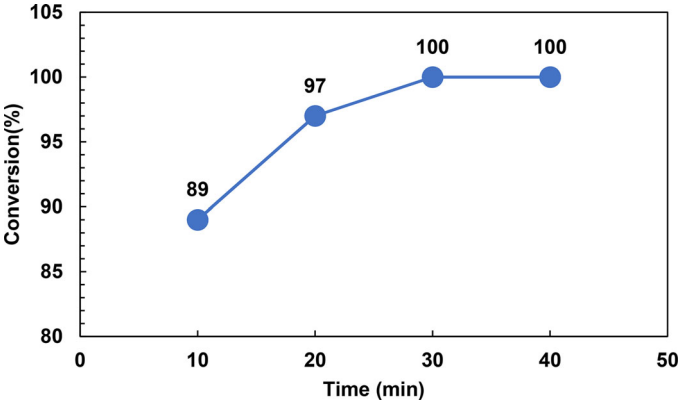

Figure 12. Effect of reaction time on oxidation rate of cyclooctene (0.5 mmol), catalyst (3.64×10^{-4} mmol), TBHP (1.5 mmol), T = 95 °C.

The N_2 adsorption-desorption isotherm of $MnFe_2O_4$ and $MnFe_2O_4$@Phttpy-MoO_2, presented in Figure 8(a,b), reveal the mesoporous characteristic of the samples. Magnetic nanoparticles show a BET surface area of 32.14 m^2g^{-1} and a total pore volume of 0.0577 cm^3g^{-1}; after anchoring the Mo complex on the nanoparticle, BET surface area and total pore volume rise to 42.45 m^2g^{-1} and 0.1499 cm^3g^{-1}, respectively.

3.2. The catalytic epoxidation of olefins by $MnFe_2O_4$@Phttpy-MoO_2

The catalytic performance of heterogeneous $MnFe_2O_4$@Phttpy-MoO_2 was investigated for selective epoxidation of various alkenes using TBHP as oxidant. First, the effects of parameters such as the amount of catalyst, kind of solvent, temperature, reaction time, the type of oxidant and also the molar ratio of oxidant/substrate were optimized. We have evaluated the catalytic behavior of $MnFe_2O_4$@Phttpy-MoO_2 in different solvents, including methanol, toluene, ethanol, dichloromethane, acetonitrile, and

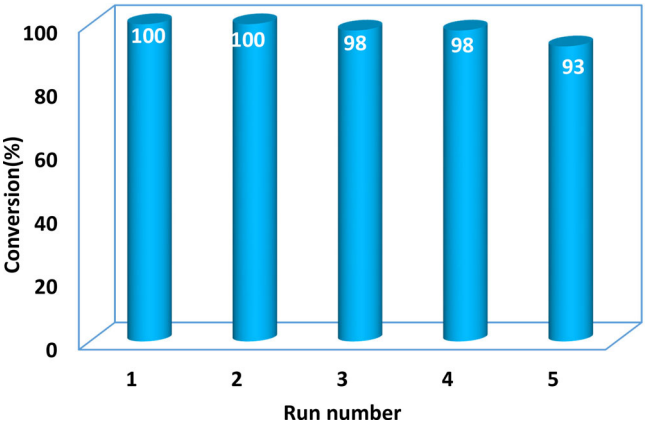

Figure 13. Reusability of $MnFe_2O_4$@Phttpy-MoO_2 in epoxidation of cyclooctene (0.5 mmol) under solvent-free conditions, TBHP (1.5 mmol), T = 95 °C.

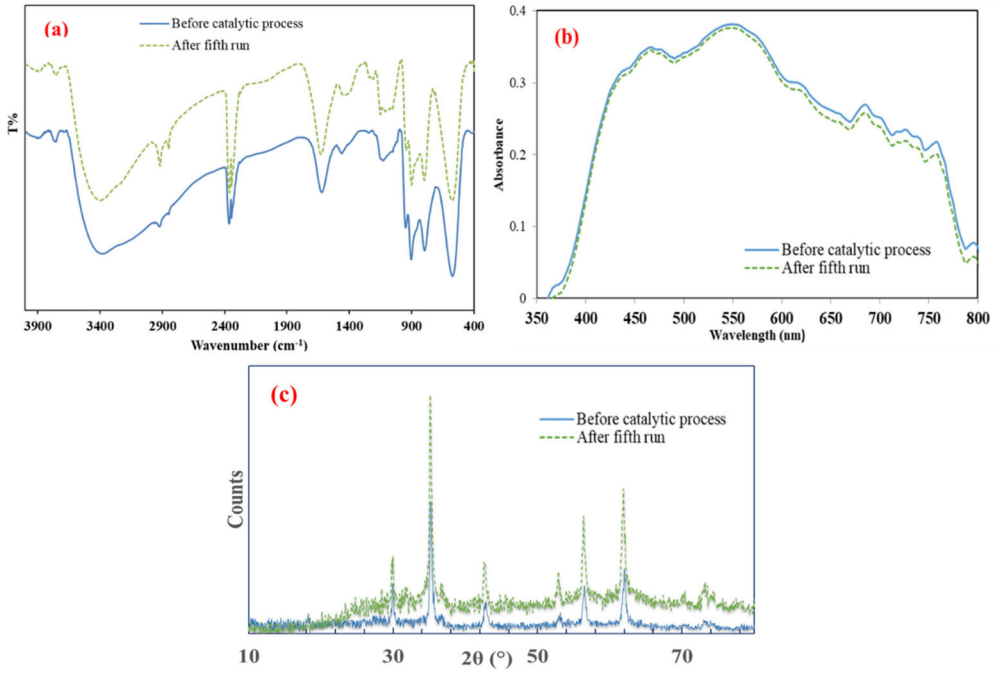

Figure 14. (a) FTIR spectra of $MnFe_2O_4$@Phttpy-MoO_2 before (solid line) and after the fifth catalytic run (dashed line). (b) DRS spectra of $MnFe_2O_4$@Phttpy-MoO_2 nanocatalyst before (solid line) and after the fifth catalytic epoxidation run (dashed line). (c) XRD pattern of $MnFe_2O_4$@Phttpy-MoO_2 nanocatalyst before (solid line) and after the fifth catalytic epoxidation run (dashed line).

chloroform. As seen in Figure 9, the best conversion of olefins to epoxides (100%) was achieved under solvent-free conditions. To assess the effect of temperature on the catalytic conversion of cyclooctene was examined. Increasing temperature of the catalytic reactor from 55 to 95 °C led to improvement of conversion percentage. As depicted in Figure 10, the highest conversion (>99%) was attained at 95 °C. Additionally, the epoxidation of cyclooctene was performed in various [TBHP]/

Table 2. Comparison of $MnFe_2O_4$@Phttpy-MoO_2 nanocatalyst and some Mo-based catalysts used for epoxidation of cyclooctene.

Entry	Catalyst	Oxidant	Time	Conversion	Ref.
1	Mo-IFNP	TBHP	2 h	96	[33]
2	Fe_2O_3@C@MoO_3	TBHP	6 h	97.3	[34]
3	MoO_x@HSS-2	TBHP	8 h	80	[35]
4	MoO_2acacen@APTS	TBHP	8 h	98	[26]
5	$[MoO_2](acac)_2$]@HAP	TBHP	2 h	95	[8]
6	RGO/Fe_3O_4@C-SalenMoO_2	TBHP	8 h	94.3	[36]
7	$MnFe_2O_4$@Phttpy-MoO_2	TBHP	30 min	$\geq$ 99	This work

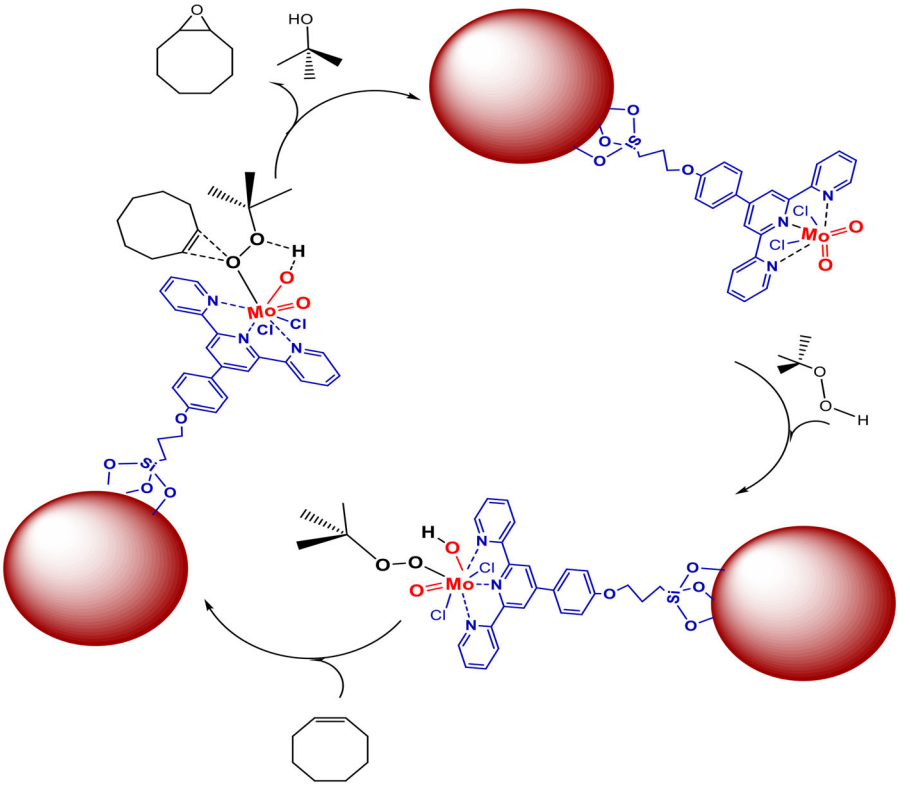

Scheme 2. Proposed mechanism for catalytic epoxidation of olefins via $MnFe_2O_4$@Phttpy-MoO_2 nanocatalyst.

[cyclooctene] ratios, 0.5, 1, 1.5, 2 and 2.5. As illustrated in Figure 11, maximum conversion was achieved in 2.0 ratio of [TBHP]/[cyclooctene]. The type of oxidant plays a major role in catalytic epoxidation of cyclooctene as a model olefin. The effects of urea-hydrogen peroxide, H_2O_2, sodium periodate and TBHP on epoxidation rates were examined. As evident from Table 1, the best epoxidation results were obtained in the presence of TBHP.

For optimization of catalyst amount, epoxidation of cyclooctene was performed under solvent-free conditions using 0.0, 1.0, 3.0, 5.0 and 7.0 mg of $MnFe_2O_4$@Phttpy-

MoO_2. The optimum catalyst amount was 5.0 mg. Ultimately the highest conversion of olefins to epoxides was achieved applying 5.0 mg of $MnFe_2O_4$@Phttpy-MoO_2, cyclooctene (0.5 mmol) as substrate, TBHP as oxidant at 95 °C under solvent-free conditions (Figure 12).

The results of catalytic epoxidation of various olefins (cyclooctene, limonene, 1-dodecene, 1-heptene, styrene, 1-indene, α-pinene, cyclohexene) under optimized conditions are presented in Table 1. The obtained results reveal high conversion (>99%) for cyclooctene, limonene, styrene and 1-dodecene using TBHP in 30 min. Also, we obtained ≥ 99 conversion and 100% epoxidation selectivity for cyclooctene under the optimum and green conditions. The propensity of internal alkenes for catalytic epoxidation is more than that of terminal ones. Hot filtration test was studied of catalyst leaching in epoxidation of cyclooctene. For this purpose, after 10 min, the catalyst was separated magnetically from the reactor with monitoring of products by gas chromatography (89% conversion). After 60 min, the products were monitored to obtain final conversion (90%) and there is no significant increase in conversion percent. This catalyst can be recycled several times without obvious changes in physical and chemical properties (Figure 13). The $MnFe_2O_4$@Phttpy-MoO_2 nanocatalyst was separated magnetically and applied five times for successive catalytic epoxidation of olefins. Comparing the FT-IR spectra (Figure 14) of the $MnFe_2O_4$@Phttpy-MoO_2 nanocatalyst before and after the fifth catalytic epoxidation run confirms the physico-chemical stability of $MnFe_2O_4$@Phttpy-MoO_2. Moreover, diffuse reflectance spectra (DRS) of $MnFe_2O_4$@Phttpy-MoO_2 before and after consecutive oxidation procedures reveals no apparent changes.

Table 2 compares the catalytic epoxidation activity of $MnFe_2O_4$@Phttpy-MoO_2 with some previously reported molybdenum based nanocatalysts in the literature. In this study, we report a magnetically recoverable heterogeneous nanocatalyst ($MnFe_2O_4$@Phttpy-MoO_2) for highly efficient epoxidation of olefins. The $MnFe_2O_4$@Phttpy-MoO_2 nanocatalyst achieved higher catalytic activity for cyclooctene epoxidation (≥99%) than other heterogeneous catalysts. Short reaction time is another important advantage of our nanocatalyst in comparison with other supported Mo catalytic systems. As expected, the catalytic epoxidation of olefins by $MnFe_2O_4$@Phttpy-MoO_2 nanocatalyst occurred through formation of a seven-coordinate intermediate (Scheme 2). The proposed mechanism consists of coordination of t-$BuOO^-$ to molybdenum(VI) as a Lewis acid center and formation of the oxoperoxomolybdenum(VI) intermediate. The next step proceeds by approach of olefin to coordinated oxygen. Finally forming a hydrogen bond between the (O) and coordinated OH, releases epoxide and alcohol from the intermediate.

4. Conclusion

Preparation of a new heterogeneous nanocatalyst based on a terpyridine based Mo(VI) complex supported on magnetic manganese ferrite nanoparticles is reported. This magnetically separable nanocatalyst showed remarkable epoxide conversion and selectivity. Furthermore, $MnFe_2O_4$@Phttpy-MoO_2 heterogeneous nanocatalyst could be applied and recovered during five runs without significant changes in its stability. The

$MnFe_2O_4$@Phttpy-MoO_2 nanocatalyst achieved higher cyclooctene conversion (≥99) and turnover frequency (2719 h^{-1}) during 30 min under green and solvent-free reaction conditions.

Disclosure statement

No potential conflict of interest was reported by the authors.

References

[1] (a) N. Mizuno, K. Yamaguchi, K. Kamata. *Coord. Chem. Rev.*, **249**, 1944 (2005). (b) Y. Shen, P. Jiang, P.T. Wai, Q. Gu, W. Zhang. *Catalysts*, **9**, 31 (2019). (c) N.A. Grosso-Giordano, C. Schroeder, A. Okrut, A. Solovyov, C. Schöttle, W. Chassé, N. Marinković, H. Koller, S.I. Zones, A. Katz. *J. Am. Chem. Soc.*, **140**, 4956 (2018). (d) S. Ghiami, M.A. Nasseri, A. Allahresani, M. Kazemnejadi. *React. Kinet. Mech. Catal.*, **126**, 383 (2019).

[2] (a) J. Zhang, P.P. Jiang, Y.R. Shen, G.H. Zhao, W.J. Zhang, G. Bian.Aust. J. Chem., **69**, 817 (2016). (b) J. Moreno, J. Iglesias, J.A. Melero, *Catalysts*, **7**, 215 (2017).

[3] (a) B. Rezazadeh, A.R. Pourali, A. Banaei, H. Behniafar. *J. Coord. Chem.*, **72**, 3401 (2019). (b) Y. Long, B. Yuan, J.T. Ma. *Chin. J. Catal.*, **36**, 348 (2015).

[4] X.B. Huang, W.C. Guo, G. Wang, M. Yang, Q. Wang, X.X. Zhang, Y.H. Feng, Z. Shi, C.G. Li. *Mater. Chem. Phys.*, **135**, 985 (2012).

[5] A. Bezaatpour, S. Khatami, M. Amiri. *RSC Adv.*, **6**, 27452 (2016).

[6] A. Bezaatpour, E. Askarizadeh, S. Akbarpour, M. Amiria, B. Babaei. *Mol. Catal.*, **436**, 199 (2017).

[7] J. Zhang, P. Jiang, Y. Shen, W. Zhang, G. Bian. *J. Porous Mater.*, **23**, 431 (2016).

[8] F. Ghanbari Resketi, S. Salehi, B. Bahramian, M. Mirzaee. *J. Phys. Org. Chem.*, **32**, e3921 (2019).

[9] M. Herbert, F. Montilla, E. Álvarez, A. Galindo. *Dalton Trans.*, **41**, 6942 (2012).

[10] R. Dileep, B. Rudresha. *RSC Adv.*, **5**, 65870 (2015).

[11] J. Sun, G. Yu, L. Liu, Z. Li, Q. Kan, Q. Huo, J. Guan. *Catal. Sci. Technol.*, **4**, 1246 (2014).

[12] A. Mavrogiorgou, M. Baikousi, V. Costas, E. Mouzourakis, Y. Deligiannakis, M. Karakassides, M. Louloudi. *J. Mol. Catal. A: Chem.*, **413**, 40 (2016).

[13] T. Chakraborty, A. Sarkar, T. Chattopadhyay. *J. Coord. Chem.*, **72**, 3430 (2019).

[14] M. Daraie, M.M. Heravi, S.S. Kazemi. *J. Coord. Chem.*, **72**, 2279 (2019).

[15] S. Dasgupta, S. Chatterjee, T. Chattopadhyay. *J. Coord. Chem.*, **72**, 550 (2019).

[16] M. Mahmoudzadeh, E. Mehdipour, R. Eisavi. *J. Coord. Chem.*, **72**, 841 (2019).

[17] M.A. Martins, C.P. Frizzo, D.N. Moreira, L. Buriol, P. Machado. *Chem. Rev.*, **109**, 4140 (2009).

[18] B. Babaei, A. Bezaatpour, H. Basharnavaz. *Polyhedron*, **179**, 114382 (2020).

[19] A. Bezaatpour, M. Amiri, V. Jahed. *J. Coord. Chem.*, **64**, 1837 (2011).

[20] M. Masteri-Farahani, S. Shahsavarifar. *Appl. Organomet. Chem.*, **32**, e4064 (2018).

[21] M.M. Foumani, A. Khorshidi, A.F. Shojaei. *ChemistrySelect*, **4**, 919 (2019).

[22] J. Rahchamani, M. Behzad, A. Bezaatpour, V. Jahed, G. Dutkiewicz, M. Kubicki, M. Salehi. *Polyhedron*, **30**, 2611 (2011).

[23] J. Mlochowski, W. Peczynska-Czoch, M. Pietka-Ottlik, H. Wójtowicz-Mlochowska. *Open Catal. J.*, **4**, 54 (2011).

[24] B. Babaei, A. Bezaatpour, M. Amiri, S. Szunerits, R. Boukherroub. *ChemistrySelect*, **3**, 2877 (2018).

[25] S. Akbarpour, A. Bezaatpour, E. Askarizadeh, M. Amiri. *Appl. Organomet. Chem.*, **31**, e3804 (2017).

[26] F. Payami, A. Bezaatpour, H. Eskandari. *Appl. Organometal. Chem.*, **32**, e3986 (2018).

[27] P. Fakhimi, A. Bezaatpour, M. Amiri, S. Szunerits, R. Boukherroub, H. Eskandari. *ChemistrySelect*, **4**, 7116 (2019).

[28] R. Ghahremanzadeh, Z. Rashid, A.H. Zarnani, H. Naeimi. *Appl. Catal. A: Gen.*, **467**, 270 (2013).
[29] O.A. Oyetade, V.O. Nyamori, B.S. Martincigh, S.B. Jonnalagadda. *RSC Adv.*, **6**, 2731 (2016).
[30] F.J. Arnaiz, R. Aguado, J.M.M. de Ilarduya. *Polyhedron*, **13**, 3257 (1994).
[31] M. Bellusci, A. La Barbera, L. Seralessandri, F. Padella, A. Piozzi, F. Varsano. *Polym. Int.*, **58**, 1142 (2009).
[32] E. Begines, C.J. Carrasco, F. Montilla, E. Álvarez, F. Marchetti, R. Pettinari, C. Pettinari, A. Galindo. *Dalton Trans.*, **47**, 197 (2017).
[33] M. Mirzaee, B. Bahramian, A. Amoli. *Appl. Organometal. Chem.*, **29**, 593 (2015).
[34] F. Zhang, H. Hu, H. Zhong, N. Yan, Q. Chen. *Dalton Trans.*, **43**, 6041 (2014).
[35] Y. Kuwahara, N. Furuichi, H. Seki, H. Yamashita. *J. Mater. Chem. A.*, **5**, 18518 (2017).
[36] Z. Li, C. Yang, Y. Ma, P. Li, J. Guan, Q. Kan. *Appl. Organometal. Chem.*, **31**, e3742(2017).